Studies of Spin-Orbit Scattering in Noble-Metal Nanoparticles Using Energy-Level Tunneling Spectroscopy

J. R. Petta and D. C. Ralph

Laboratory of Atomic and Solid State Physics, Cornell University, Ithaca, New York 14853

(Received 21 June 2001; published 6 December 2001)

The effects of spin-orbit scattering on discrete electronic energy levels are studied in copper, silver, and gold nanoparticles. Level-to-level fluctuations of the effective g-factor for Zeeman splitting are characterized, and the statistics are found to be well described by random matrix theory predictions. The strength of spin-orbit scattering increases with atomic number and also varies between nanoparticles made of the same metal. We compare the spin-orbit scattering rates in the nanoparticles to weak-localization measurements on larger samples.

DOI: 10.1103/PhysRevLett.87.266801 PACS numbers: 73.22.–f, 72.25.Rb, 73.23.Hk

Spin-orbit (SO) interactions are central to determining the energy-level structure of atomic nuclei, large-atomic-number atoms, and solid-state systems. They affect electronic band structures [1], they influence the symmetry class of random-matrix theories applied to quantum systems [2], and they are put to use in proposals for manipulation of electron spins [3]. A particularly fundamental method for probing SO interactions in solid-state systems is to examine individual quantum energy levels in nanoparticles, both because SO matrix elements can be measured directly and because SO interactions produce strong modifications of the effective g-factors for spin-Zeeman splitting. Previously, measurements of three individual energy levels in gold nanoparticles showed that SO effects reduce the g-factor to $g \sim 0.28-0.45$ [4], in contrast with Al particles, which ordinarily give $g \approx 2$ [5]. Adding 4% gold to an aluminum nanoparticle also increased the SO scattering [6]. In this paper we report systematic studies of SO effects in noble-metal nanoparticles covering a range of atomic number (Z)—copper, silver, and gold. We characterize the mesoscopic fluctuations, present within single particles, of the g-factors and SO matrix elements $\langle H_{\mathrm{so}} \rangle$, and find that the statistics for the g-factors are well described by recent predictions of random-matrix theory (RMT) [7,8]. From the values of the g-factors and the mean energy-level spacing δ [9], we extract SO scattering rates for each material, assuming that effects of spin magnetic moments are dominant, and we find order of magnitude agreement with expectations based on weak-localization measurements.

SO interactions cause the electronic energy levels in a metal grain to be not purely spin-up or spin-down, and as a consequence they reduce the g-factor for spin-Zeeman splitting below the free-electron value of 2. In low-Z nanoparticles for which SO scattering is sufficiently weak (with $\langle H_{\mathrm{so}} \rangle \ll \delta$) perturbation theory can be used to calculate the g-factor for a given electronic state n [10]:

$$g_n = 2\left(1 - 2\sum_{m \neq n} \frac{|\langle \Psi_{m\downarrow} | H_{\mathrm{so}} | \Psi_{n\uparrow} \rangle|^2}{(E_n - E_m)^2}\right). \qquad (1)$$

Here the Ψ_m denote the unperturbed (pure-spin) single-electron eigenstates with energy E_m. It is expected that the SO matrix elements will vary between different pairs of unperturbed energy levels because they depend on the precise nature of the wave functions, which are chaotic and fluctuating [11]. The local energy-level spacing will also vary. As a result, g_n should exhibit mesoscopic fluctuations for different levels, n. For heavier elements, perturbation theory ceases to be valid. However, for large SO-interaction strengths, Brouwer *et al.* and Matveev *et al.* have recently employed RMT to predict the statistical distribution $P(g)$ of g-factors in a nanoparticle [7,8,12]. In [7], the strength of SO interactions is tuned continuously, allowing numerical studies of the full crossover from the Gaussian orthogonal ensemble to the Gaussian symplectic ensemble for the energy-level statistics. In this crossover, it is found that the mean value of $P(g)$ shifts to smaller g-factors and the variance of the distribution exhibits a maximum for $\langle g \rangle \sim 1.2$.

Our tunneling samples are fabricated in a vertical geometry through a 3–10 nm bowl-shaped hole etched in a Si_3N_4 membrane [5,13] (see inset, Fig. 1). One electrode is made by evaporating 1750 Å of Al on top of the membrane to fill the bowl. Following oxidation in 50 mTorr of O_2 for 3 min to form a tunnel barrier, 5–20 Å of Cu, Ag, or Au is evaporated on the lower side of the device to form approximately hemispherical particles with radii of 3–5 nm. A second tunnel barrier is then formed by the evaporation of 11 Å of Al_2O_3. This is followed by 1750 Å of Al to make the lower tunneling electrode. The samples are screened at 4.2 K to select those whose current-voltage (I-V) curves exhibit Coulomb-staircase steps, indicating tunneling through a single nanoparticle. Then more detailed I-V curves are measured in a dilution refrigerator, with all electrical leads passing through copper-powder filters to minimize the effects of rf radiation.

Figure 1 shows I-V and dI/dV-V curves for a Cu device (Cu #1). As V is increased, I increases in discrete steps due to tunneling through well-resolved energy levels within the nanoparticle [5]. The resonances in the differential conductance correspond to the energy-level spectrum of the nanoparticle. In an applied magnetic field (H) most resonances in dI/dV divide into two peaks, allowing

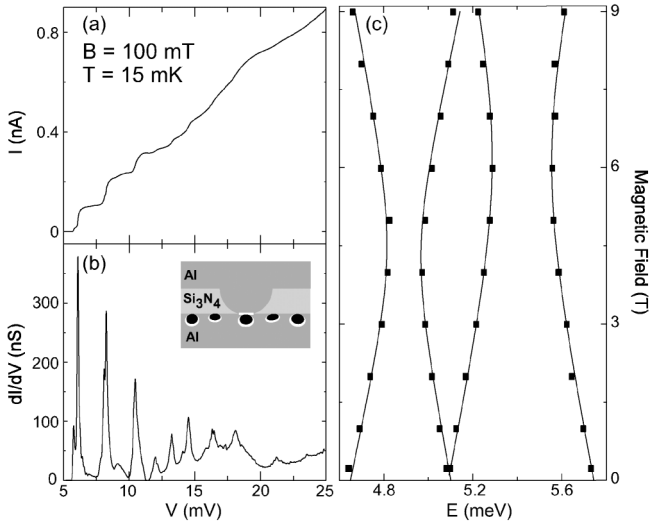

FIG. 1. (a) I-V and (b) dI/dV-V curves for Cu #1. (c) Magnetic field dependence of peaks in dI/dV for energy levels exhibiting avoided level crossings. The V scale has been converted to energy, using the procedure discussed in the text. Inset: Cross-sectional device schematic. Throughout the paper, the magnetic field is in the plane of the Si_3N_4 film.

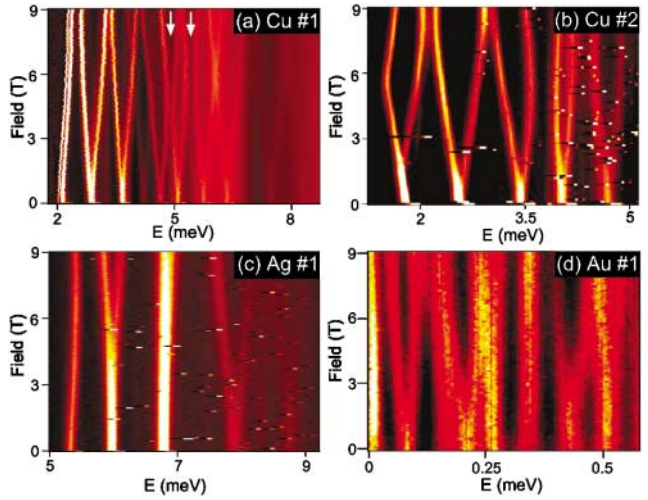

FIG. 2 (color). Color scale plots of dI/dV in (a) and (b) Cu, (c) Ag, and (d) Au samples as a function of energy and magnetic field. The arrows denote the avoided crossings of Fig. 1.

measurements of the energy difference for spin-Zeeman splitting between Kramers-pair eigenstates, $\Delta E = g\mu_B H$. In order to determine the effective g-factors, we must convert the magnitude of the splitting from the measured value in voltage to energy, correcting for capacitive division of the voltage across the two tunnel junctions according to $\Delta E = \Delta V/(1 + C_1/C_2)$ where C_1/C_2 is the capacitance ratio for the two tunnel junctions. This ratio can be determined by measuring the shift in V for the resonances as the aluminum leads are changed from superconducting to normal in small magnetic fields, or by comparing the voltage for tunneling through the same quantum state for positive and negative V [5]. The low-field g-factors for sample Cu #1 fall in the range from 1.30 ± 0.04 to 1.82 ± 0.05.

In the weak SO-scattering limit where perturbation theory is valid, the effects of SO interactions on the magnetic field evolution of neighboring energy levels [shown in detail in Fig. 1(c) and in broader view in Fig. 2(a)] can be modeled by diagonalizing a simple 2×2 Hamiltonian matrix with off-diagonal matrix elements $\langle H_{so}\rangle$ coupling the eigenstates [6]. The minimum energy difference at the avoided level crossing gives $2\langle H_{so}\rangle$ between those two states. The solid lines in Fig. 1(c) correspond to solutions of 2×2 Hamiltonians with $\langle H_{so}\rangle = 76$ μeV for the avoided crossing near 4.9 meV, and $\langle H_{so}\rangle = 134$ μeV for the avoided crossing near 5.4 meV. These matrix elements are in the size range expected based on the measured g-factors and the mean level spacing $\delta = 0.70$ meV. If the level spacing were uniform and equal to this value, and all the matrix elements $\langle H_{so}\rangle$ were $\sim$130 μeV, then Eq. (1) would predict a typical value $g = 2 - 6.6(\langle H_{so}\rangle/\delta)^2 \sim 1.77$. If level-spacing fluctuations are included, the estimate for the average value of $2 - g$ is modified by a few percent [8].

For the heavier elements Ag and Au, the g-factors become smaller with increasing atomic number. Figure 2 shows color scale plots of dI/dV for increasing magnetic field in Cu, Ag, and Au samples. We find g-factors in the range 1.3 to 1.9 for Cu, 0.25 to 1.1 for Ag, and 0.05 to 0.19 in Au for the samples shown. Table I lists the measured mean values of the g-factors and their standard deviations for all the samples we have measured with more than three resolvable resonances.

The most direct way to compare the statistics of the measured g-factors with theoretical predictions is by plotting the integrated probability distribution of the g-factors for each sample. In Fig. 3 the points correspond to the g-factors from several Au, Ag, and Cu samples, while the solid lines are the theoretical predictions from Brouwer *et al.* [7] with the SO-scattering strength parameter λ adjusted to minimize the least squares error between the theoretical and experimental distributions. Our results are in

TABLE I. Sample parameters. N is the number of resonances resolved, $\langle g\rangle$ is the mean g-factor, $\sigma_e(g)$ is the experimental standard deviation, $\sigma_t(g)$ is the standard deviation of the theory curve with the best-fit value of the SO parameter λ as defined in [7], δ is the mean level spacing, and $1/\tau_{so}$ is the spin-orbit scattering rate calculated as discussed in the text.

	N	$\langle g\rangle$	$\sigma_e(g)$	$\sigma_t(g)$	λ	δ(meV)	$1/\tau_{so}(s^{-1})$
Cu #1	9	1.58	0.20	0.17	0.7	0.70	2×10^{11}
Cu #2	5	1.22	0.30	0.31	1.2	0.71	5×10^{11}
Cu #3	5	0.79	0.29	0.29	2.1	0.36	8×10^{11}
Ag #1	5	0.69	0.34	0.27	2.4	0.85	2×10^{12}
Ag #2	5	1.54	0.07	0.17	0.7	1.13	3×10^{11}
Au #1	7	0.12	0.06	0.05	12.7	0.10	8×10^{12}
Au #2	7	0.17	0.07	0.07	9.5	0.12	5×10^{12}
Au #3	5	0.45	0.27	0.18	3.9	0.27	2×10^{12}

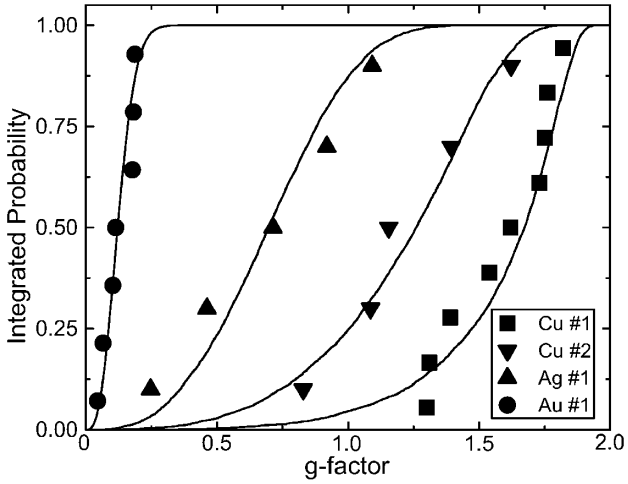

FIG. 3. Integrated probability distributions of the g-factors for several samples (points), compared to the predictions of random-matrix theory with the SO-interaction strength adjusted for the best fit (lines). See Table I for the sample parameters.

good qualitative agreement with the RMT predictions. In particular, for a single value of the adjustable parameter λ, the theoretical distributions account reasonably for both the mean value of g and the standard deviation for each sample.

We do observe significant differences in the average value of the g-factor for different nanoparticles composed of the same material, e.g., for the two Cu samples depicted in Fig. 3 and for the Ag samples #1 and #2. This is true even though the mean level spacings for the two Cu samples are nearly identical. Because of these differences, we cannot meaningfully consolidate the data from many samples to improve the quality of our statistics in making comparisons to the RMT predictions. The physical origin of SO interactions at low temperatures within noble metal nanoparticles is expected to be scattering from defects or the nanoparticle surface [14–16]. Sample-to-sample variations in the strength of SO interactions are therefore reasonable in nanoparticles, if the defect concentration or the surface-to-volume ratio may vary, for instance, due to size and shape differences between particles.

A few of the energy levels shown in Fig. 2 do not exhibit Zeeman splitting. We observe this only in samples where we can identify the tunneling transitions as corresponding to changes from an odd to an even number of conduction electrons within the particle. We make this identification by observing the lowest energy tunneling resonance. If the nanoparticle initially has an odd number of electrons, then the first energy level accessible for tunneling will have only one spin state available, and therefore the lowest energy transition does not undergo Zeeman splitting [Figs. 2(a), 2(c), and 2(d)] [5]. In other words, the tunneling transition occurs via a spin-singlet state. Similarly, we can explain the lack of observed splitting in some higher energy resonances as due to tunneling via excited spin-singlet states. [See the states near 7 meV in Fig. 2(c) and 0.3 meV in Fig. 2(d).] It is also possible that the Zeeman splitting may sometimes be sufficiently small for a level in Ag or Au that we cannot resolve it. Our resolution limit is approximately $g \geq 0.03$. From the theoretical probability distributions of Fig. 3, about 0.02% of the states in Ag and 1.4% of the states in Au can be expected to have $g < 0.03$.

In some samples, background-charge noise and nonequilibrium effects can interfere with accurate determinations of the statistics of the g-factors. For instance, as a function of the voltage across the device or as a function of time, the background charge affecting the nanoparticle can sometimes take on an ensemble of different values, shifting the energy levels that one is trying to measure. When this happens, current steps due to background-charge changes may be misinterpreted as due to quantum states, or the same quantum state may be measured several times at different values of voltage. In one Cu sample not shown in this paper, we measured six apparently different resonances all with an identical g-factor of 1.50, which we ascribe to this effect. This behavior was not seen in any other samples measured in this study. If several closely spaced levels are observed in a sample, ways to diagnose the cause as background noise include the presence of negative differential conductance even with normal-state electrodes, the presence of apparent level crossings rather than avoided crossings, and identical g-factors for several resonance peaks.

An important question for understanding the properties of nm-scale devices is whether the strength of SO scattering is consistent with expectations based on measurements made by other techniques on larger samples, or whether there is new physics at small scales. Because effective g-factors measured by different experimental techniques can probe physically distinct quantities [8], we will make the comparison based on estimates for SO scattering times (τ_{so}) that we can extract from our data. In the limit of strong SO scattering in a nanoparticle, the g-factor is predicted to have contributions from both spin and orbital magnetic moments, so that it depends separately on τ_{so} and the mean free path l [8,9]:

$$\langle g^2 \rangle = \frac{3}{\pi \hbar}\, \tau_{so} \delta \,+\, \alpha \frac{l}{L}\,, \qquad (2)$$

with $\alpha \approx 1$ for a spherical particle and L the particle size. Studies of lattice fringes in TEM for Au test samples indicate that our nanoparticles are not disordered—a majority are single crystals, while 20%–30% possess a grain boundary. We therefore do not expect l to be much smaller than L. As a result, Eq. (2) predicts that $\langle g^2 \rangle$ for Au nanoparticles should never be much less than 1. This is in conflict with our measurement of $\langle g^2 \rangle$ as small as 0.019 for Au #1. In the following, we will consequently put aside the orbital-moment term $\alpha l/L$ in Eq. (2), and explore what values of τ_{so} result by assuming that only the first term due to the spin magnetic moment is significant. For the Au samples, using the values of δ listed in Table I, we find $1/\tau_{so} = (2\text{–}8) \times 10^{12}\ \mathrm{s}^{-1}$. The Ag and Cu samples

fall outside the strong-scattering regime for which Eq. (2) applies. However, by fitting the measured g-factors to the numerical distributions calculated by Brouwer *et al.,* we can still determine τ_{so} for each sample from the single fitting parameter λ defined in [7]: $1/\tau_{so} = \lambda^2\delta/(\pi\hbar)$. This formula also ignores the contribution of any orbital magnetic moment to g. By this method, the SO scattering rates determined for the two Ag samples are quite different, $1/\tau_{so} = 3 \times 10^{11}$ s^{-1} and 2×10^{12} s^{-1}, while for Cu $1/\tau_{so} = (2\text{–}8) \times 10^{11}$ s^{-1}.

For Cu, we can also use perturbation theory to check the rate determined from the RMT approach. The value of τ_{so} within perturbation theory is [17]

$$1/\tau_{so} = \frac{2\pi|\langle H_{so}\rangle|^2}{\hbar\delta}. \quad (3)$$

For $\langle H_{so}\rangle \sim 130$ μeV and $\delta = 0.7$ meV appropriate for Cu #1, we find $1/\tau_{so} \sim 2 \times 10^{11}$ s^{-1}, in agreement with the rate for Cu #1 listed in Table I.

These values for τ_{so} can be compared to the SO scattering rates determined by weak localization measurements on quench-condensed noble-metal films [18]. We compare to these data because the mean free paths of the quench-condensed films are comparable to the size of our nanoparticles, so that the scattering contribution to SO-induced spin relaxation [14,16] should be similar. Bergmann [18] found $1/\tau_{so} = 5.4 \times 10^{12}$ s^{-1} for Au, $(2.6\text{–}3.1) \times 10^{11}$ s^{-1} for Ag (depending on the disorder), and 3.2×10^{11} s^{-1} for Cu. The values for Au and Cu agree to within a factor of 3 with all the rates we extract, while the weak-localization rate for Ag coincides with sample Ag #2 but not Ag #1.

In conclusion, we have measured the g-factor distributions in Cu, Ag, and Au nanoparticles using tunneling spectroscopy. The g-factors within a given sample exhibit mesoscopic fluctuations, with distributions in good accord with random-matrix-theory predictions. We have observed significant differences in both the g-factor distributions and τ_{so} between different nanoparticles composed of the same metal, illustrating the importance of the specific sample structure in the origin of SO scattering. The small g-factors we measure for Au particles do not indicate a large contribution from orbital magnetic moments in the regime of strong SO scattering. However, if we assume that the physics governing the g-factors is dominated by spin-magnetic-moment physics, the SO scattering rates that we extract for the nanometer-scale particles are in order-of-magnitude agreement with weak localization measurements.

We thank P. Brouwer, K. Matveev, C. B. Murray, and X. Waintal for discussions and assistance. This work was supported by the Packard Foundation and the NSF (DMR-0071631 and a Graduate Research Fellowship). Sample fabrication was performed at the Cornell node of the National Nanofabrication Users Network.

[1] N. W. Ashcroft and N. D. Mermin, *Solid State Physics* (Holt, Rinehart and Winston, Philadelphia, 1976).
[2] C. W. J. Beenakker, Rev. Mod. Phys. **69**, 731 (1997).
[3] S. Datta and B. Das, Appl. Phys. Lett. **56**, 665 (1990).
[4] D. Davidović and M. Tinkham, Phys. Rev. Lett. **83**, 1644 (1999).
[5] D. C. Ralph, C. T. Black, and M. Tinkham, Phys. Rev. Lett. **74**, 3241 (1995).
[6] D. G. Salinas, S. Gueron, D. C. Ralph, C. T. Black, and M. Tinkham, Phys. Rev. B **60**, 6137 (1999).
[7] P. W. Brouwer, X. Waintal, and B. I. Halperin, Phys. Rev. Lett. **85**, 369 (2000).
[8] K. A. Matveev, L. I. Glazman, and A. I. Larkin, Phys. Rev. Lett. **85**, 2789 (2000).
[9] We define δ as the mean spacing between Kramers' doublets at $H = 0$. This is the same definition used in [7], but it is twice the level spacing defined in [8].
[10] J. Sone, J. Phys. Soc. Jpn. **42**, 1457 (1977).
[11] M. L. Mehta, *Random Matrices* (Academic Press, San Diego, 1991).
[12] Effects in bulk samples have been considered by A. Y. Zyuzin and R. A. Serota, Phys. Rev. B **45**, 12 094 (1992).
[13] K. S. Ralls, R. A. Buhrman, and R. C. Tiberio, Appl. Phys. Lett. **55**, 2459 (1989).
[14] R. J. Elliott, Phys. Rev. **96**, 266 (1954).
[15] Y. Yafet, in *Solid State Physics,* edited by F. Seitz and D. Turnbull (Academic, New York, 1963), Vol. 14.
[16] For a recent review, see J. Fabian and S. Das Sarma, J. Vac. Sci. Technol. B **17**, 1708 (1999).
[17] W. P. Halperin, Rev. Mod. Phys. **58**, 533 (1986).
[18] G. Bergmann, Z. Phys. B **48**, 5 (1982).